



Retrieval of tropospheric NO₂ columns from satellite measurements in presence of cirrus: A theoretical sensitivity study using SCIATRAN and prospect application for the A-Train

Jérôme Vidot^{a,*}, Olivier Jourdan^a, Alexander A. Kokhanosvsky^b, Frédéric Szczap^a, Vincent Giraud^a, Vladimir V. Rozanov^b

^a Laboratoire de Météorologie Physique (LaMP), Université Blaise Pascal, OPGC/CNRS, 24 avenue des Landais, Aubière F-63177, France

^b Institute of Environmental Physics (IUP), Institute of Remote Sensing (IFE), University of Bremen, Otto-Hahn-Allee 1, Bremen D-28359, Germany

ARTICLE INFO

Article history:

Received 24 March 2009

Received in revised form

18 October 2009

Accepted 19 October 2009

Keywords:

Cirrus properties

OMI

Tropospheric NO₂ vertical column

SCIATRAN

A-train

ABSTRACT

A theoretical sensitivity study of the influence of cirrus cloud properties on tropospheric NO₂ columns retrieved from the spaceborne Ozone Monitoring Instrument (OMI) measurements is performed. It is conducted within the framework of the synergetic use of A-Train sensors to derive more representative trace gas products. We aim to study the potential effects of cirrus clouds on tropospheric NO₂ retrievals using a retrieval algorithm that, unlike the OMI Standard and DOMINO algorithms, does not correct for the effects of clouds. The sensitivity study is based on the radiative transfer code SCIATRAN that performs both simulations of top of atmosphere (TOA) reflectances as measured by an OMI-like band and tropospheric NO₂ column retrievals based on the differential optical absorption spectroscopy (DOAS) method. The results of the sensitivity study show that if a correction for cirrus clouds is not included in our simple retrieval that does not account for clouds in the first place, the tropospheric column can be underestimated by 55%. This underestimation depends strongly on cirrus parameters as, in order of importance, cloud fraction, cloud optical depth, asymmetry factor of cirrus cloud phase function and cloud top height. The perspective of the synergy between OMI and cloud information obtained from cloud-derived products of the A-Train is evaluated in two parts by applying a simple cloud correction scheme based on the independent pixel approximation (IPA). Firstly, we evaluated the tropospheric NO₂ column retrievals error caused by uncertainties in cirrus cloud properties. Secondly we studied the influence of subpixel cloud optical depth variability on NO₂ retrievals. From our simulations, it is demonstrated that the error will be reduced significantly if the cloud fraction is lower or equal to 0.5. In this case, the cloud fraction and the cloud optical depth must be known within accuracy less than 0.05% and 50%, respectively. The cloud top height and the asymmetry factor must be known within uncertainty of at least 1 km and less than 0.05, respectively. The latter result shows that the uncertainty of the asymmetry factor is a major source of error in the cloud correction for tropospheric NO₂ retrieval in the presence of cirrus.

© 2009 Elsevier Ltd. All rights reserved.

1. Introduction

Nitrogen dioxide (NO₂) plays an important role in the tropospheric chemistry [1]. NO₂ is known to be one of the key species in the formation of photochemical smog

* Corresponding author. Tel.: +33 473405276; fax: +33 473405136.
E-mail address: J.Vidot@opgc.univ-bpclermont.fr (J. Vidot).

during pollution episodes. In the troposphere, the concentration of NO_2 takes part in the chemical budget of ozone. It also contributes to acid rain and locally, to radiative forcing over industrial regions and urban areas [2]. To assess accurately our current knowledge of tropospheric chemistry and its interaction with climate, global information about the amounts and distribution of NO_2 is required. By their high spatial and temporal coverage, satellite measurements of NO_2 are essential for air quality monitoring (for health regulation) and regional scale modelling (improvement of emission estimates).

The measurement of tropospheric NO_2 from space began with the precursor satellite Global Ozone Monitoring experiment (GOME) [3] followed by the Scanning Imaging Absorption Spectrometer for Atmospheric Cartography (SCIAMACHY) [4] and the Ozone Monitoring Instrument (OMI) [5]. The retrieval algorithms of the NO_2 vertical columns are based on the differential optical absorption spectroscopy (DOAS) approach [6]. This technique is based on the analysis of differential structure of backscattered signal using nonlinear least squares fitting in a specific wavelength window. The spectral fit determines a slant column density of NO_2 which is converted into a vertical column by application of an air mass factor (AMF). Retrievals of tropospheric NO_2 columns from GOME, SCIAMACHY and OMI have demonstrated the weekly cycle of NO_2 [7], its relationship with NO_x emission, the annual trend over industrial countries [8], the global cartography of tropospheric NO_2 [9] and the diurnal evolution of NO_2 driven by emissions and photochemistry [10]. Space-based measurements of NO_2 have been validated against ground-based measurements [11,12], atmospheric models [13,14] and aircraft measurements [9,15].

Nevertheless, the retrieval of NO_2 from space measurements can be subject to significant errors. Boersma et al. [16] showed that NO_2 tropospheric vertical column can only be retrieved with an accuracy of 35–60%. The retrieval errors are dominated by uncertainties in the tropospheric AMF. The *a priori* NO_2 profile shape, the surface albedo and the cloud properties (especially cloud fraction) are the leading sources of errors associated with AMF computation. Moreover, clouds cover approximately 60% of the earth's surface. Hence, considering the weak spatial resolutions of trace gas monitoring sensors (for GOME: $320 \times 40 \text{ km}^2$, SCIAMACHY: $60 \times 30 \text{ km}^2$ and OMI: $13 \times 24 \text{ km}^2$ at nadir), more than 90% of their measurements are contaminated by clouds [17].

The effects of clouds on trace gas retrieval from space measurements can be separated into three parts [18–22]. The first effect, called shielding effect, reduces the interaction between photons and trace gas underneath the cloud leading to an “apparent” decrease of depths of absorption lines. The second effect, called albedo effect, increases the depth of absorption lines of the gas layer above the cloud as compared to the clear sky. This is due to enhanced single and multiple scattering light paths from Sun to cloud to satellite. The third effect, called in-cloud absorption, increases the depth of absorption lines of gas layer inside the cloud. Here, light scattering process due to the cloud is responsible for the light path enhancement as compared to a nonscattering layer. These three effects are competing

together and the final effect depends on the cloud properties as well as on the profile of the trace gas. Therefore, accurate space-based retrievals of trace gas column in presence of clouds necessarily imply a precise assessment of the cloud radiative and macrophysical properties which are, in turn, determined by their microphysical, optical and geometrical characteristics.

The most important point to perform a cloud correction for the retrievals of tropospheric NO_2 column is to identify the cloud parameters that significantly modify the depth of absorption lines of NO_2 . Studies of Boersma et al. [16] and Wang et al. [23] showed that the cloud fraction, cloud albedo and cloud pressure were important quantities for cloud correction. Errors in these cloud properties will directly end up in errors in NO_2 columns. However the quantitative estimate of the retrieval errors depends on the chosen cloud model. For OMI, the cloud correction scheme of the current algorithm is based on the simplified Lambertian cloud model that assumes a homogeneous cloud with an albedo of 0.8 [24]. This method corrects the cloud contribution of the total reflectance at the top of atmosphere (TOA) measured for an OMI pixel using only two cloud parameters: the effective cloud fraction and cloud pressure. The use of this Lambertian cloud model compared to a scattering cloud model has been estimated to lead to AMF differences between –10% and 10% [23] and mean AMF differences of –12% with a standard deviation of 10% [25], depending on cloud properties, cloud fraction and NO_2 pollution. However, the assumption of a Lambertian cloud model is only valid if the bi-directional properties of light reflectance from clouds can be neglected.

In order to overcome these limitations, the cloud correction algorithm can be improved on the basis of collocated data from cloud sensors and gas sensors onboard different satellites. The A-train satellite constellation allows for near simultaneous measurements of cloud and trace gas properties at different spatial scales. For instance, high spatial resolution (typically $(1 \times 1 \text{ km}^2)$) cloud properties can be assessed from the Moderate Resolution Imaging Spectroradiometer (MODIS) [26] and from the 5-km resolution cloud product provided by the Cloud–Aerosol Lidar with Orthogonal Polarization (CALIOP) (Level 2 Algorithm Theoretical Basis Document, available at: http://www-calipso.larc.nasa.gov/resources/pdfs/PC-SCI-202_Part4_v1.0.pdf). This subpixel cloud information (cloud cover, optical thickness, cloud top height...) can then be used to constrain a cloud correction algorithm applied to OMI measurements. Nevertheless, the use of CALIOP information is limited by the fact that CALIOP only overlaps with the nadir pixel of OMI.

This paper lies within the framework of using the synergy of A-Train instruments to improve trace gas retrievals in presence of cirrus clouds. Due to their low optical thickness, cirrus clouds are more difficult to detect compared to cumulus, particularly over land and ice surfaces. Additionally, infrared measurements have shown that thin cirrus clouds (with optical depths between 0.1 and 1.0) have a global frequency of about 20–40% [27]. More recently, a cirrus occurrence up to 70% near the tropics over the 100–180°E longitude band has been

derived from active measurements by CALIOP [28]. From these observations, this paper aims at studying into the potential effects of cirrus clouds on the tropospheric NO₂ column retrievals from OMI space-based measurements and the impact of uncertainties in cirrus cloud properties in a cloud correction scheme based on the IPA. It is important to point out that this study is focusing on the effect of cirrus clouds properties in the NO₂ absorption band and that the results presented here are not compared with the operational cloud correction scheme of OMI that is based on the O₂–O₂ absorption band [24]. Even if we can assume that the O₂–O₂ band is sensitive to cirrus, the OMI O₂–O₂ algorithm will retrieve, in situations of cirrus, a small value for effective cloud fraction and high cloud height. For small cloud fractions, the assumption on the surface albedo plays an important role and will impact the retrieval of tropospheric NO₂ column. This effect is beyond the scope of the paper, but the new surface albedo database made from OMI itself [29] will certainly change the tropospheric NO₂ retrievals, because the previous albedo database was from GOME with a coarser pixel than OMI.

Theoretical sensitivity study of the inversion of the tropospheric NO₂ column to undetected or retrieved (with errors) cirrus cloud properties is discussed in this paper. The sensitivity study is based on radiative transfer model (RTM) simulations of TOA reflectances as measured in an OMI-like band. The first part of the paper will describe the atmospheric model, the retrieval algorithm and the cirrus cloud model. In the second part of the paper, the results of the sensitivity study that highlight the cirrus parameters that influence tropospheric NO₂ column retrievals are presented. The last part is devoted to the perspective on application of A-Train cloud-derived products by estimating tropospheric NO₂ column error caused by uncertainties in cirrus cloud parameter or caused by subpixel cloud optical depth inhomogeneity within an OMI pixel at nadir.

2. NO₂ retrieval algorithm and model setups

2.1. Atmospheric model

In our study, the atmosphere is treated as plane-parallel. In the spectral band used by OMI for NO₂ retrieval (between 405 and 465 nm), the two other trace gases, namely O₃ and H₂O are included with fixed standard atmospheric profiles. The collision complex of oxygen molecules O₂–O₂ is included as well by assuming a fixed standard atmospheric profile of O₂. The influence of cirrus clouds is evaluated in different tropospheric NO₂ situations characterized by the three atmospheric profiles of NO₂ volume mixing ratio (VMR in ppbv) shown in Fig. 1. The NO₂ VMR profile represented by the full line corresponds to the lowest NO₂ contribution in the troposphere whereas the NO₂ VMR profile represented by the dotted-dashed line corresponds to the largest NO₂ contribution. The tropospheric part of the total atmospheric NO₂ vertical column is commonly retrieved by assuming that the longitudinal variation of the stratospheric NO₂ vertical column is small. Therefore, tropospheric NO₂ vertical column (V_{tr}) over a polluted location (e.g., over a city) can

be retrieved from the total NO₂ vertical column by removing the total NO₂ vertical column over a clean site (e.g., Pacific ocean) at a given location with the same latitude. Here, we simply removed a constant stratospheric NO₂ vertical column from the total vertical column. The stratospheric NO₂ vertical column was calculated as the integral of the NO₂ profile from 12 km to the top of atmosphere (TOA). Accordingly, the three profiles displayed in Fig. 1 correspond to three tropospheric NO₂ conditions defined as: (1) low polluted with $V_{tr}=0.43 \times 10^{15}$ mol/cm² (full line), (2) moderately polluted with $V_{tr}=2.81 \times 10^{15}$ mol/cm² (dotted line) and, (3) heavily polluted with $V_{tr}=9.36 \times 10^{15}$ mol/cm² (dotted-dashed line).

The modelling results presented in this paper are performed for single values of the surface albedo $A=0.05$, the solar zenith angle $\theta_s=30^\circ$ and the viewing zenith angle $\theta_v=0^\circ$ (according to OMI nadir viewing geometry). The influence of the solar angle and the surface albedo are discussed in Section 3. We note in passing that aerosols were chosen to be not included in the atmospheric model.

2.2. DOAS retrieval

The tropospheric NO₂ vertical column (V_{tr}) retrieval algorithm has been developed in the framework of SCIATRAN [30]. SCIATRAN is both a radiative transfer code and a retrieval algorithm for many atmospheric gases (see <http://www.iup.uni-bremen.de/sciattran/> for full description of SCIATRAN). For the retrievals of V_{tr} , the DOAS technique is applied to simulated TOA reflectance in the OMI-like band with a spectral sampling of 0.21 nm [31] and with a signal to noise ratio (SNR) of 1400 [10]. Retrievals of V_{tr} are performed by converting the simulated TOA reflectances R_{TOA} to so-called differential optical densities D , which are calculated as

$$D(\lambda) = \ln(R_{TOA}(\lambda)) - P_3(\lambda), \quad (1)$$

where $P_3(\lambda)$ is a third degree least squares polynomial fit of the logarithm of R_{TOA} with respect to the wavelength λ , that removes slowly varying functions. The conversion of R_{TOA} into D ensures the better contrast of the NO₂ absorption line depths to improve the accuracy of the fitting procedure. Then, in the retrieval algorithm the quadratic form

$$F(\lambda, V_{tr,ret}) = \|D_{true}(\lambda, V_{tr,true}) - D_{ret}(\lambda, V_{tr,ret})\|^2, \quad (2)$$

is minimized with respect to unknown parameter $V_{tr,ret}$. D_{true} is the differential optical density spectrum simulated with SCIATRAN for the true tropospheric NO₂ column $V_{tr,true}$. D_{ret} is the retrieved differential optical density spectrum for the retrieved tropospheric NO₂ column $V_{tr,ret}$.

2.3. Cirrus cloud model

Cirrus clouds are treated as single layer homogeneous clouds. The most important cirrus cloud parameters that potentially influence the trace gas retrieval are those which determine the photon paths in the atmosphere. In the visible spectral range, these parameters are expected to be the cloud optical depth τ , the cloud phase function P , the

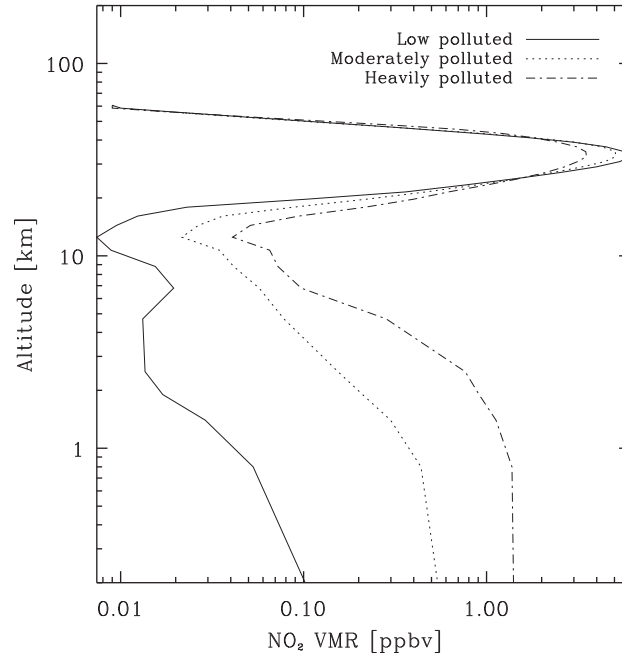


Fig. 1. Atmospheric profiles of NO_2 volume mixing ratio in ppbv used in the study.

cloud top height z and the cloud geometrical depth h [32]. These parameters are used as inputs in SCIATRAN. Because of the quite large spatial resolution of OMI measurement ($13 \times 24 \text{ km}^2$), one more important parameter is the geometric cloud fraction c . In most retrieval, c is accounted for considering the independent pixel approximation (IPA). IPA consists in the hypothesis that R_{TOA} is the sum of the reflectance of a cloudy part (R_{cloudy}) and the reflectance of a clear-sky part (R_{clear}) as

$$R_{\text{TOA}} = cR_{\text{cloudy}} + (1 - c)R_{\text{clear}}. \quad (3)$$

The ice crystals phase function used for SCIATRAN simulations has been retrieved from in situ aircraft measurements during the Cirrus Cloud Experiment (CIRCLE2) campaign. The phase function (Fig. 2) was inferred from the polar nephelometer (PN) measurements. The best fit of the PN measurements was achieved using a combination of spherical ice particles with diameters ranging from 1 to $100 \mu\text{m}$ and rough droxtal shaped particles with maximum dimension between 2 and $200 \mu\text{m}$. Accordingly, two particle size distributions were retrieved using the iterative inversion method developed by Oshchepkov et al. [33] and upgraded by Jourdan et al. [34]. Then, the scattering patterns of the retrieved particle size distribution were computed with the Lorenz–Mie theory (for spherical particles) and with an improved geometric-optics model (for droxtal particles) at a wavelength of 420 nm [35]. The retrieved phase function exhibits a featureless behaviour and is flat at side scattering angles which is in accordance with most of the observations [33,34,36–38] or scientific recommendations in ice cloud remote sensing application [39–42]. The corresponding asymmetry factor g is 0.75.

To illustrate the influence of cirrus clouds on the retrieval of V_{tr} , Fig. 3 shows simulated differential optical densities

(calculated with Eqs. (1) and (3)) with and without cirrus clouds. R_{clear} is calculated using SCIATRAN with standard profiles of O_3 , H_2O and O_2 , surface albedo and geometries described in Section 2.1. Clouds properties ($\tau=1$, CIRCLE2 phase function, $z=10 \text{ km}$ and $h=1 \text{ km}$) are added in the calculation of R_{cloudy} . The heavily polluted NO_2 profile is considered. The clear-sky differential optical density ($c=0$ in Eq. (3)) is represented by the green line. Blue and red lines represent differential optical densities when a cirrus cloud is included and cover the full pixel ($c=1$) and half of the pixel ($c=0.5$), respectively. When a cirrus cloud is included, the depths of NO_2 absorption lines are reduced. This stems from the cloud shielding effect discussed in the introduction, which is greater to both cloud albedo and in-cloud absorption effects. Because V_{tr} varies with the NO_2 absorption lines depths, the presence of undetected cirrus would lead to a lower apparent V_{tr} , that depends on the cloud fraction. Nevertheless, these results are valid for algorithms that do not make any attempt to correct for clouds in the first place. In the current available OMI NO_2 algorithms such as the OMI standard retrieval [43] and the Dutch OMI NO_2 (DOMINO) retrieval [44], the missing tropospheric NO_2 column due to clouds is compensated by adding a ghost column obtained from chemical transport model. In situations of cirrus, the OMI $\text{O}_2\text{--O}_2$ algorithm will retrieve a small value for effective cloud fraction and high cloud height. Because of the small effective cloud fraction, the ghost column effect will also be small.

3. Influence of undetected cirrus clouds on NO_2 retrieval

The differential optical densities simulated previously are used to introduce the following discussion that focuses on the influence of undetected cirrus cloud on

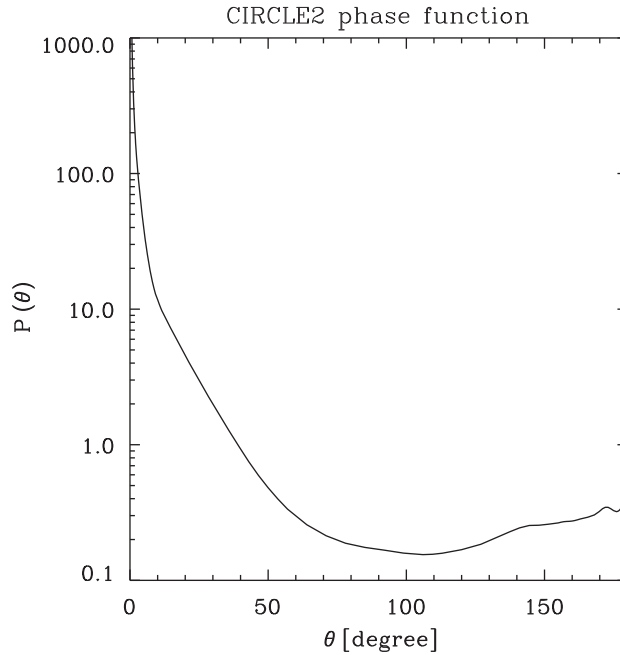


Fig. 2. Cirrus cloud phase function inferred from aircraft measurement during the CIRCLE2 campaign.

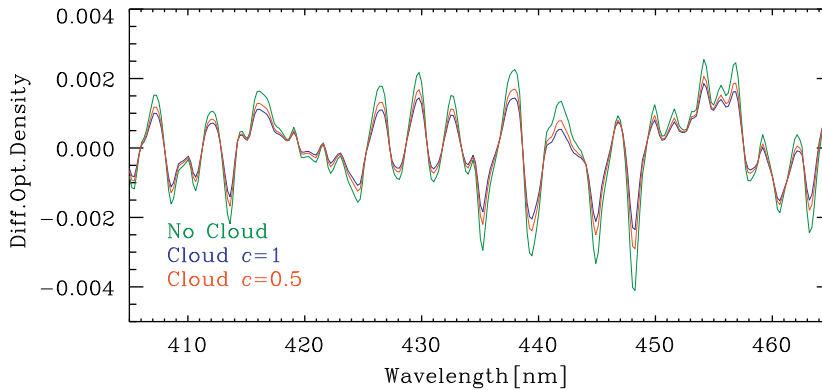


Fig. 3. Differential optical densities for heavily polluted troposphere without cloud (green line), with $c=1$ (blue line) or $c=0.5$ (red line). (For interpretation of the references to colour in this figure legend, the reader is referred to the webversion of this article.)

the tropospheric NO_2 column retrieval. The influence of undetected cirrus clouds is evaluated as an error on the retrieved tropospheric NO_2 column $V_{tr,ret}$ compared to a true tropospheric NO_2 column $V_{tr,true}$:

$$\text{Error} = \frac{V_{tr,ret} - V_{tr,true}}{V_{tr,true}} \times 100, \quad (4)$$

$V_{tr,ret}$ is retrieved according to the following methodology: A true TOA reflectance spectrum is calculated following Eq. (3), for an atmosphere characterized by both a cirrus cloud with prescribed properties and a true tropospheric NO_2 column $V_{tr,true}$. Then, this TOA reflectance is used as the input spectrum for the DOAS-based SCIATRAN retrieval algorithm. The retrieved quantity is, in that case, called $V_{tr,ret}$. It is important to point out that the inversion procedure is performed with the hypothesis of a non-cloudy atmosphere. By this mean, errors caused by a

specific cirrus parameter (optical depth, cloud top height, etc....) can be quantified and used to determine the relative importance of the impact of a given cloud parameter on the retrieval of tropospheric NO_2 columns for retrievals that do not correct for clouds in the first place.

3.1. Cloud fraction and cloud optical depth

The panel of Fig. 4 displays errors of the retrieved $V_{tr,ret}$ as a function of cloud optical depth and cloud fraction for low polluted condition (Fig. 4a), for moderately polluted condition (Fig. 4b) and for heavily polluted condition (Fig. 4c). For these cases, $z=10$ km, $h=1$ km and $g=0.75$ (i.e., with the CIRCLE2 ice crystal phase function). The overall negative error (underestimation) highlights the predominance of the shielding effect. This is explained by the

fact that the tropospheric NO_2 is mainly situated under the cirrus cloud. Even for the highest value of the cloud optical depth considered in this study ($\tau=3$), the albedo effect still remains negligible compared to the shielding effect. The underestimation of $V_{\text{tr,ret}}$ increases rapidly with both τ and c and can reach, for $\tau=3$ and $c=1$, an underestimation of $\sim 35\%$ in low polluted conditions

(Fig. 4a), $\sim 45\%$ in moderately polluted conditions (Fig. 4b) and $\sim 55\%$ in heavily polluted condition (Fig. 4c). It is interesting to notice that the underestimation remains less than 5% for optical depth less than 0.2 whatever the cloud fraction and the polluted conditions are. This implies, from our simulations, that optically thin cirrus or subvisible cirrus do not significantly influence the NO_2

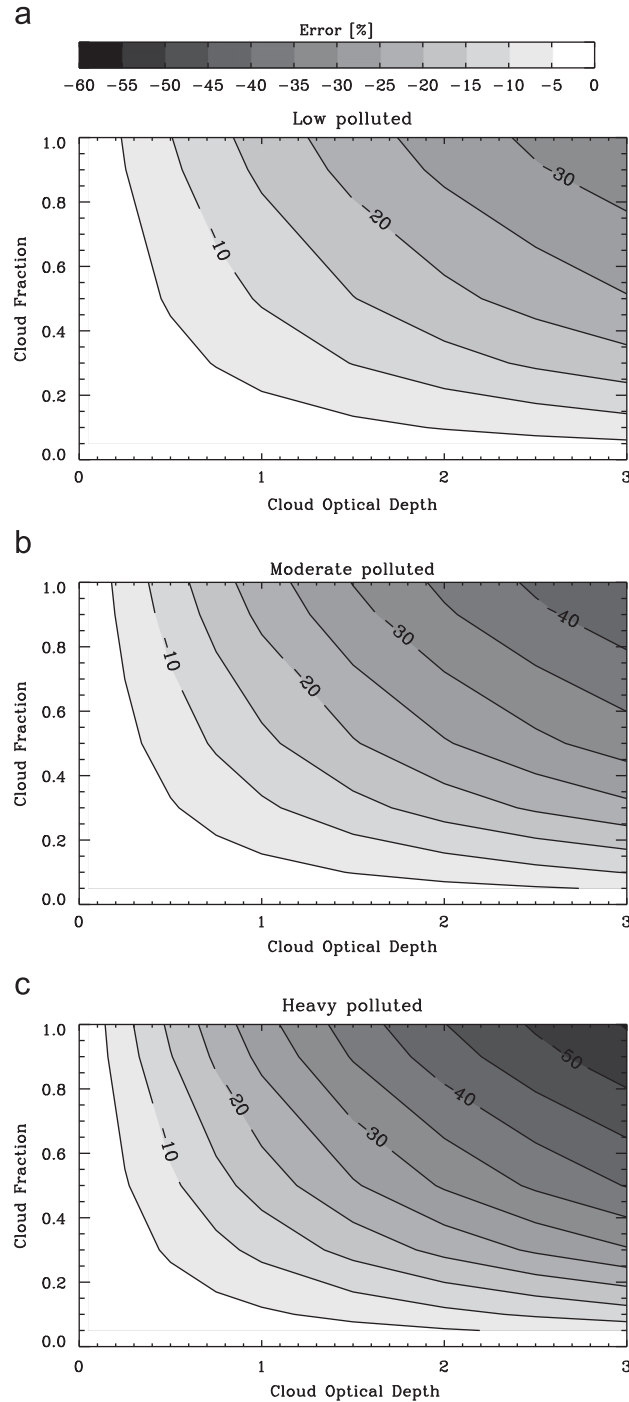


Fig. 4. NO_2 tropospheric error caused by undetected cirrus cloud as function of cloud optical depth and cloud fraction. Here, $z=10$ km, $h=1$ km and $g=0.75$: (a) low polluted; (b) moderate polluted; (c) heavy polluted.

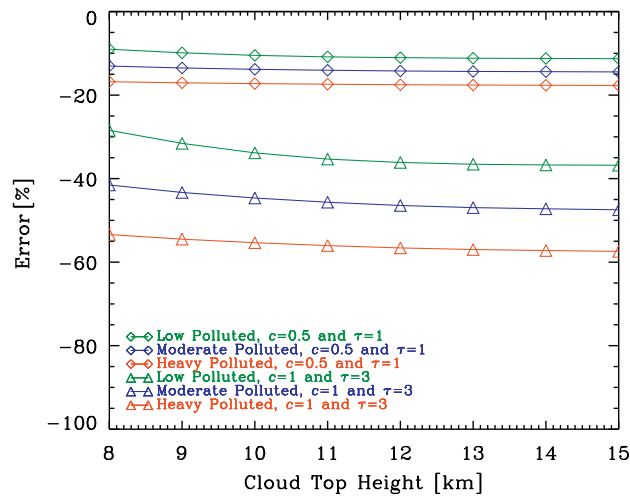


Fig. 5. NO₂ tropospheric error caused by undetected cirrus cloud versus cloud top height. Green, blue and red lines stand for low, moderately and heavily polluted conditions. Cloud fraction and cloud optical depth were assumed to be 0.5 and 1, respectively for diamonds and to be 1 and 3 for triangles. Here, $h=1$ km and $g=0.75$. (For interpretation of the references to color in this figure legend, the reader is referred to the webversion of this article.)

Table 1

NO₂ tropospheric error difference caused by cloud top height z variability.

Error difference (%) between $z=8$ and 15 km	$\tau=0.05$	$\tau=1$	$\tau=3$
$c=0.05$	0.01	0.29	1.07
	0.01	0.18	0.78
	0.01	0.12	0.56
$c=0.5$	0.10	2.26	6.15
	0.06	1.40	4.39
	0.09	0.90	3.03
$c=1$	0.19	3.63	8.35
	0.12	2.20	5.93
	0.17	1.35	4.02

Values in each box of fixed c and τ correspond to low, moderately and heavily polluted conditions, respectively.

tropospheric column retrieval which is not the case for example, in atmospheric CO₂ retrieval [45,46]. This might be explained by the fact that, in the NO₂ absorption band, the signal is predominantly due to Rayleigh scattering as compared to CO₂ absorption band that is in the near infrared spectral band and where the Rayleigh scattering is very low.

3.2. Cloud top height and cloud geometrical depth

The influence of cloud top height (z) and cloud geometrical depth (h) is evaluated in terms of error difference between the maximum and the minimum NO₂ tropospheric column errors over the different values of z and h considered. Fig. 5 displays the error caused by undetected cirrus clouds versus cloud top height z . In these simulations, $g=0.75$ and $h=1$ km. Colour lines and symbols differ with pollution conditions, cloud fraction and cloud optical depth. For $c=1$ and $\tau=3$ in low polluted condition (represented by the green line with triangles),

the error is -29% at $z=8$ km and -37% at $z=15$ km leading to an error difference of 8% between $z=8$ and 15 km. As comparison, the error difference is $\sim 6\%$ for moderately polluted condition (represented by the blue line with triangles) and $\sim 4\%$ for heavily polluted condition (represented by the red line with triangles). The underestimation increase with cloud top height mostly between $z=8$ and 12 km. This is explained by the increase of shielding effect with the altitude of the cirrus cloud. For $c=0.5$ and $\tau=1$ (represented by lines with diamonds), error differences are almost constant with z . Table 1 provides a summary of error differences for different values of c and τ . Errors remain less than 1% for low optical depth ($\tau=0.05$) or for low cloud fraction ($c=0.05$). We noticed also that, for fixed c and τ , error differences decrease with polluted conditions, which can be explained by an increase of the in-cloud absorption effect when the cloud is lower due to higher tropospheric NO₂ (see Fig. 1). The error caused by undetected cirrus clouds versus cloud geometrical depth h is represented in Fig. 6 for the same cases as Fig. 5. Underestimation of V_{tr} decrease slowly with h due to increase of in-cloud absorption leading to error difference of few percents between $h=0.1$ and 2 km. Table 2 provides a summary of error differences for different values of c and τ which, overall, remain less than 3%.

3.3. Asymmetry factor of ice crystal phase function

The influence of ice crystal phase function is evaluated by comparing the retrieval errors versus the asymmetry factor g . g is used to parameterize the general behaviour of the ice crystal phase function because it is an integrated optical parameter (scalar) taking into account both ice crystals shape and size variability. The different values of asymmetry factor tested here are obtained on the basis of nine pre-calculated phase functions for different ice crystal shape (aggregate, plate, column, bullet and dendrite) and effective diameters comprise between 4.5

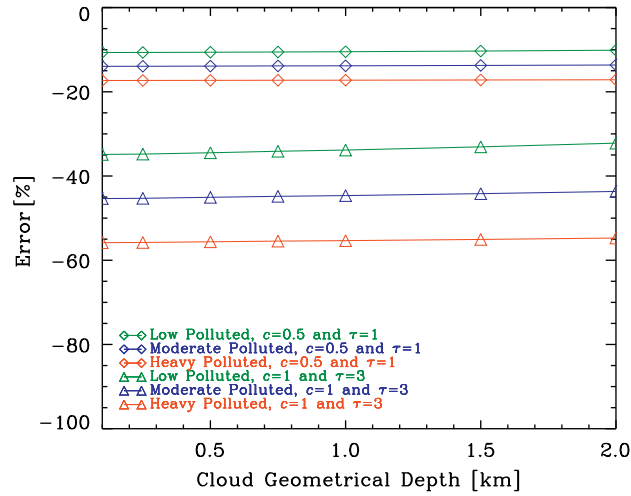


Fig. 6. Same as Fig. 5 versus cloud geometrical depth. Here, $z=10$ km and $g=0.75$.

Table 2

Same as Table 1 for cloud geometrical depth h .

Error difference (%) between $h=0.1$ and 2 km	$\tau=0.05$	$\tau=1$	$\tau=3$
$c=0.05$	0.01	0.08	0.34
	<0.01	0.04	0.21
	<0.01	0.02	0.14
$c=0.5$	0.03	0.54	1.96
	0.02	0.31	1.23
	0.02	0.17	0.81
$c=1$	0.05	0.88	2.69
	0.04	0.49	1.69
	0.04	0.27	1.10

and $150\mu\text{m}$ that are used for cirrus clouds modelling [47]. The CIRCLE-2 phase function is included as well. The asymmetry factor values obtained are between 0.70 and 0.85. Errors caused by undetected cirrus clouds versus asymmetry factors are displayed in Fig. 7. It appears that the underestimation decreases with the asymmetry factor. This is explained by the fact that cirrus cloud particles with a large value of g reflect less solar radiation than ice crystals with smaller asymmetry factor. Then, for a large value of g , more solar radiation exhibited by the cirrus cloud will interact with tropospheric NO_2 located below the cloud. From the summary given in Table 3, error differences between $g=0.70$ and 0.85 are comprised between 0.07% (for $c=0.05$, $\tau=0.05$ and low polluted condition) and 21.3% (for $c=1$, $\tau=3$ and heavily polluted condition). These results imply that, for fixed c and τ , the error difference caused by undetected cirrus clouds with g lying between 0.70 and 0.85 (Table 3) is more important than the one caused by undetected cirrus clouds with z comprised between 8 and 15 km (Table 1) or h comprised between 0.1 and 3 km (Table 2). The asymmetry factor appears to be a major source of error in tropospheric NO_2 retrieval in the presence of cirrus.

This sensitivity study showed that four cirrus parameters influence the retrieval of tropospheric NO_2 columns. These parameters are, in descending order, the cloud fraction c , the cloud optical depth τ , the asymmetry factor g and the cloud top height z . Since the error difference caused by cloud geometrical depth variability remains less than 3%, we have considered that cloud geometrical depth does not influence significantly the retrieval of tropospheric NO_2 columns. The $V_{tr,ret}$ errors have also been estimated for other solar zenith angles (15° , 45° and 60°) and other surface albedos (0.03 and 0.1) but they do not show large discrepancies with the results obtained for a solar zenith angle of 30° and a surface albedo of 0.05.

4. Error on NO_2 retrieval caused by uncertainties in cirrus clouds properties

The next step of our study is to look at the $V_{tr,ret}$ error induced by uncertainties of the cirrus parameters that were identified previously as critical. The objective here is to evaluate the precision needed for these parameters in order to constrain the retrievals. To this respect, we simulated a true R_{TOA} using Eq. (3) with a set of cirrus properties (τ , g , z , h), a cloud fraction c and a true tropospheric NO_2 vertical column $V_{tr,true}$. Then, $V_{tr,ret}$ is obtained by using as the input reflectance spectrum for the inversion algorithm, the clear-sky part of the TOA reflectance R_{clear} . R_{clear} is a function of $R_{TOA}(p)$ and $R_{cloud}(p+\delta p)$ where p is τ , g , z , h or c . The formulation of R_{clear} is presented for each cloud parameters in the following subsections. Results are presented for moderately polluted condition as results found for the three polluted conditions did not differ significantly.

4.1. Cloud fraction

The error on tropospheric NO_2 column retrievals caused by uncertainty in cloud fraction is calculated as

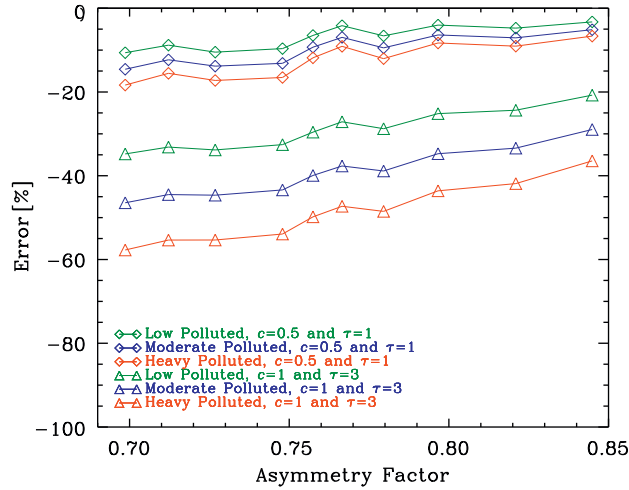


Fig. 7. Same as Fig. 5 versus asymmetry factor. Here, $z=10$ km and $h=1$ km.

Table 3

Same as Table 1 for asymmetry factor g .

Error difference (%) between $g=0.65$ and 0.85	$\tau=0.05$	$\tau=1$	$\tau=3$
$c=0.05$	0.07	1.00	2.66
	0.07	1.29	3.40
	0.09	1.61	4.21
$c=0.5$	0.66	7.37	12.25
	0.77	9.44	15.40
	0.89	11.69	18.85
$c=1$	1.27	11.30	14.04
	1.52	14.24	17.50
	1.76	17.58	21.27

Eq. (4). The input reflectance spectrum of the inversion scheme is defined as

$$R_{\text{clear}} = \frac{R_{\text{TOA}}(\tau, g, z, h, c) - (c + \delta c)R_{\text{cloud}}(\tau, g, z, h)}{1 - (c + \delta c)}, \quad (5)$$

where δc is the uncertainty on cloud fraction. The simulations were performed for a cirrus cloud characterized by an asymmetry factor of 0.75, a cloud top height of 10 km and a geometrical thickness of 1 km. The surface albedo, solar zenith angle and the viewing angle are the same as in Section 3. Fig. 8 displays errors on $V_{\text{tr,ret}}$ versus cloud optical depth for $\delta c=0.01$ (Fig. 8a), $\delta c=0.05$ (Fig. 8b) and $\delta c=0.09$ (Fig. 8c) and for three values of c (0.1, 0.5 and 0.8) representing low, medium and high cloud fractions. Overall, the overestimation of cloud fraction results in an overestimation of tropospheric NO_2 columns (i.e., positive errors). If $c \leq 0.5$ (represented by lines with triangles or diamonds), overestimations are expected to be less than 10% if $\delta c \leq 0.05$ (Figs. 8a and b) and less than 20% if $\delta c=0.09$ (Fig. 8c). If $c \geq 0.8$, overestimations are expected to be higher, ranging from 10% to more than 100%, if $\delta c \geq 0.05$ (Figs. 8b and c) for large cloud optical depth ($\tau > 1$).

Within the framework of combining measurements performed by A-train sensors to improve OMI NO_2

products, cloud fraction can be derived from independent measurements. For example, MODIS can provide a sub-pixel cloud fraction information with a $1 \times 1 \text{ km}^2$ resolution. Accordingly, the cloud fraction estimation from MODIS within an OMI pixel is expected to be achieved with lower uncertainty than the value of 0.05 reported by Koelemeijer et al. [48]. However, the estimation of the uncertainty on MODIS cloud fraction is a difficult task because it depends on the cloud type. Koren et al. [49] reported that for small cumulus cloud, MODIS cloud fraction is almost twice as the cloud fraction obtained from a finer spatial resolution (30 m) instrument. Fortunately, cirrus clouds have larger spatial extension than small cumulus clouds and would be less influenced by the scale dependence. Finally, these results highlight that cloud fraction within an OMI pixel should be determined with uncertainty lower than 0.05 in order to reduce the tropospheric NO_2 vertical columns errors, especially if the cloud optical depth is greater than 1.

4.2. Cloud optical depth

The error on tropospheric NO_2 columns retrieval caused by uncertainties in the cloud optical depth is calculated as Eq. (4) where the retrieval is applied on the clear-sky part of the reflectance given by

$$R_{\text{clear}} = \frac{R_{\text{TOA}}(\tau, g, z, h, c) - cR_{\text{cloud}}(\tau + \delta\tau, g, z, h)}{1 - c}, \quad (6)$$

where $\delta\tau$ is the uncertainty in cloud optical depth. The simulations were performed for a cirrus cloud characterized by $g=0.75$, $z=10$ km and $h=1$ km. The panel of Fig. 9 displays errors on V_{tr} versus cloud optical depth for $\delta\tau/\tau=10\%$ (Fig. 9a), $\delta\tau/\tau=20\%$ (Fig. 9b) and $\delta\tau/\tau=50\%$ (Fig. 9c) and for three values of c (0.1, 0.5 and 0.8, differentiated by symbols). Here again, the overestimation of cloud optical depth results in an overestimation of tropospheric NO_2 columns. This is explained by the fact that an overestimation of τ will increase the cloud reflectance. The numerator of Eq. (6) will then decrease

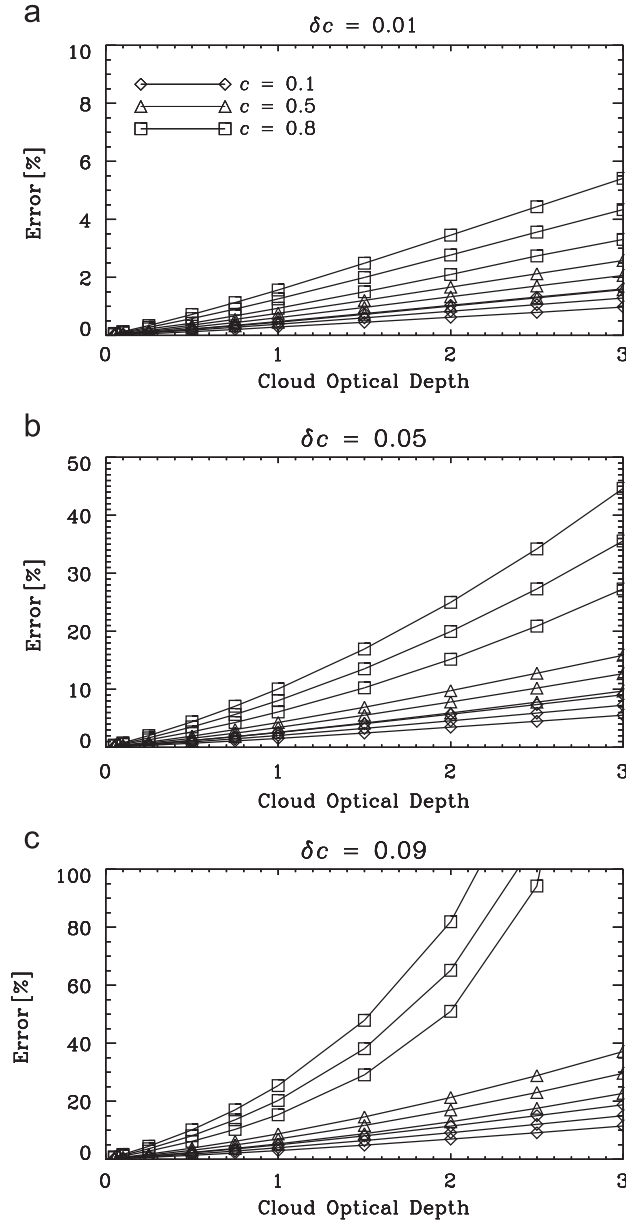


Fig. 8. NO₂ tropospheric column error caused by an uncertainty in the cloud fraction (a) $\delta c = 0.01$, (b) $\delta c = 0.05$ and (c) $\delta c = 0.09$ versus cloud optical depth and for different cloud fraction ($c = 0.1, 0.5$ and 0.8 , differentiated by symbols). Here, $z = 10$ km, $h = 1$ km and $g = 0.75$ and moderately polluted condition is assumed.

leading to an overestimation of tropospheric NO₂ columns. For $c \leq 0.5$, overestimations are expected to be less than 15% if $\delta\tau/\tau \leq 20\%$ (Figs. 9a and b). The same result is seen if $\delta\tau/\tau = 50\%$ and $\tau < 1$ (Fig. 9c). If $c = 0.8$, overestimations are expected to increase quickly, especially if $\delta\tau/\tau = 50\%$ (Fig. 9c).

By comparison, cirrus optical depth from MODIS and ground-based measurement has shown that MODIS overestimates the optical depth by 30% [50]. However, clouds with low optical depth (less than 0.4) are not retrieved from MODIS [51]. The use of CALIOP data will be helpful for a better characterization of the optical depth since CALIOP

is able to detect clouds with $\tau < 0.05$ [52]. Nevertheless, the use of CALIOP information is limited by the fact that CALIOP only overlaps with the nadir pixel of OMI. If no CALIOP data is available and the cirrus cloud is undetected by MODIS (i.e., $\tau < 0.4$), tropospheric NO₂ vertical column errors are expected to be less than 10% (Fig. 4).

4.3. Asymmetry factor

The error on tropospheric NO₂ columns retrieval caused by uncertainties in asymmetry factor is retrieved from the clear-sky part of the reflectance given by Eq. (6) and where

the uncertainty is applied to g instead of τ . Here again, g was chosen instead of the phase function because it is a convenient integrated parameter function of the ice particle shape and effective size. So it is a first guess indicator of the general scattering behaviour of the cirrus cloud. Fig. 10 displays errors versus cloud optical depth. R_{TOA} is simulated with $g=0.75$, $z=10$ km and $h=1$ km. Here, the overestimation of asymmetry factor results in an underestimation of tropospheric NO_2 columns (i.e., negative errors). Underestimations up to 40% are expected if $c=0.5$ (full lines) and up to 60% if $c=0.8$ (dashed lines), but do not change that much whether $\delta g=0.05$ (diamonds) or $\delta g=0.1$ (triangles). These results show that the uncertainty of the asymmetry factor is a major source of error in

tropospheric NO_2 retrieval in the presence of cirrus. However, although modelling studies show that for ice crystals values of g could vary from 0.7 to 0.9 (see for instance the review of Baran [53]), measurements do not show such variability in ice clouds. An uncertainty less than 0.05 can be expected since the asymmetry factor ranges more likely from 0.75 to 0.80 for ice clouds and from 0.80 to 0.85 for mixed phase clouds depending on the liquid water fraction [54,55]. However, the operational algorithms of MODIS retrieve the ice crystals effective radius (R_{eff}) and not g . Both information on R_{eff} and shape are needed to model the scattering properties of ice crystals. Usually, a combination of particles with different shapes and sizes is used as an equivalent microphysical model in MODIS

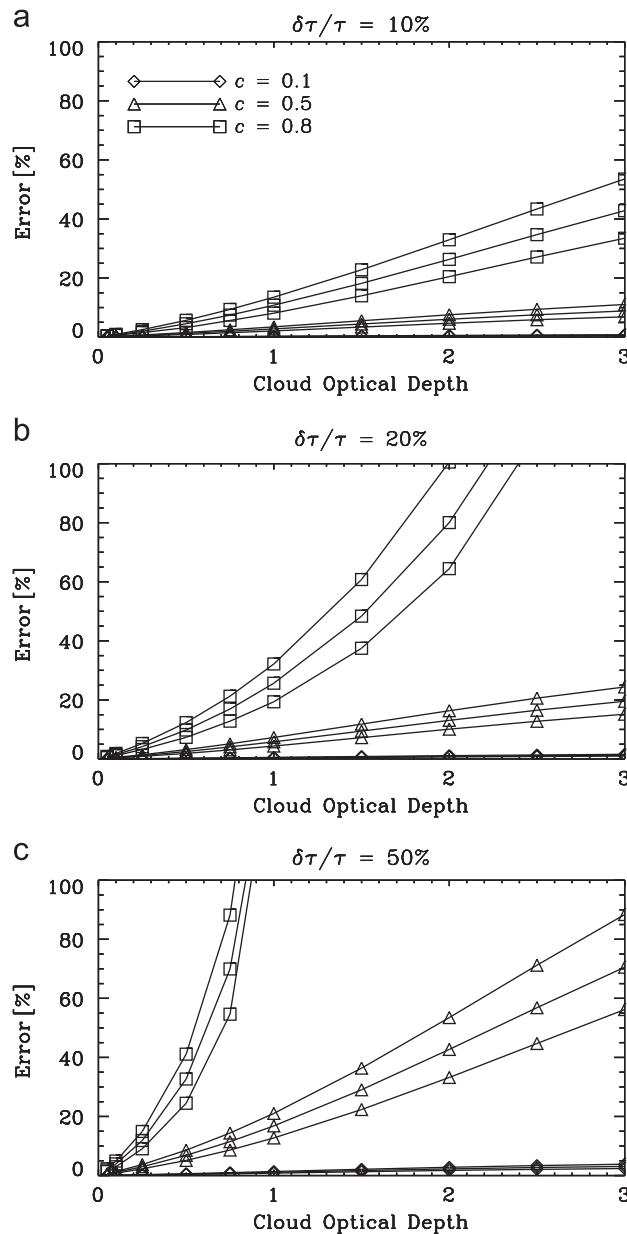


Fig. 9. Same as Fig. 8 for (a) $\delta\tau/\tau=10\%$, (b) $\delta\tau/\tau=20\%$ and (c) $\delta\tau/\tau=50\%$.

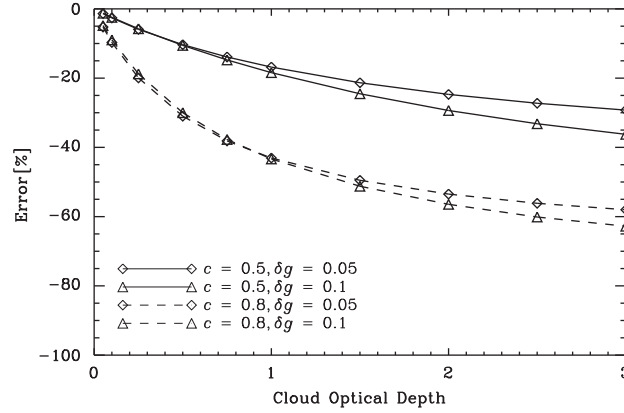


Fig. 10. NO₂ tropospheric column error caused by an uncertainty in the asymmetry factor $\delta g=0.05$ (diamonds) and $\delta g=0.1$ (triangles) versus cloud optical depth for $c=0.5$ (full lines) and $c=0.8$ (dashed lines). Here, $z=10$ km, $h=1$ km and $g=0.75$ and moderate polluted condition is assumed.

retrieval process of the effective radius. The retrieved R_{eff} from MODIS corresponding to a specific microphysical shape model could be used to assess appropriate phase function and asymmetry parameter on the basis of MODIS look-up-tables (LUT) [56,57]. However, MODIS R_{eff} seems to be overestimated by comparison with Lidar retrievals [58].

4.4. Cloud top height

The error on tropospheric NO₂ column retrievals caused by uncertainties in the cloud top height is assumed from the clear-sky part of the reflectance given by Eq. (6) and where the uncertainty is applied on z instead of τ . The panel of Fig. 11 displays errors on V_{tr} versus cloud optical depth for $\delta z=0.5$ km (Fig. 11a), $\delta z=1$ km (Fig. 11b) and $\delta z=3$ km (Fig. 11c) and for two values of c (0.5 and 0.8) and three values of z (8, 10 and 12 km). If $\delta z \leq 1$ km (Figs. 11a and b), errors are expected to be less than 20%. If $\delta z=3$ km (Fig. 11c), errors are expected to be less than 20% if $c \leq 0.5$. Uncertainty of z retrieved from MODIS is currently under investigation but preliminary results by comparison with Lidar measurements show difference on the order of 1 km [58]. However, this comparison remains limited due to the high occurrence of multi-layers ice clouds where MODIS only retrieves an effective cloud top height. The use of CALIOP retrieval will allow constraining the cloud top height input in order to retrieve the tropospheric NO₂ column in presence of cirrus cloud.

5. Contribution of subpixel cloud optical depth

The IPA formulation of the TOA reflectance in presence of clouds given by Eq. (3) does not consider the subpixel inhomogeneity of cloud properties. To this respect, we can consider that the optical thickness can be derived more accurately from high spatial resolution measurements (1×1 km²) of MODIS. This information will be used to describe the variability of the optical thickness within an OMI pixel (13×24 km²). Therefore, two ways of determining the contribution of the cloud to the total reflectance measured by OMI can be considered: (1) by calculating R_{cloud} from the mean cloud optical depth $\langle \tau \rangle$ or (2) by

calculating the mean cirrus cloud reflectance $\langle R_{cloud} \rangle$ corresponding to a distribution of optical depth within an OMI pixel. These two ways of calculating the contribution of the cloud would have an important impact on the computing time of the retrieval because in the first way, there is only one calculation for the mean cloud optical depth whereas in the second way there are several calculations for each value of the subpixel cloud optical depth distributions. To compare these two ways, we have simulated different distribution of cloud optical depth considering a gamma distribution. Nine distributions have been selected randomly with three mean cloud optical depths ($\langle \tau \rangle=0.5, 1$ or 2) and three variances ($v_\tau=0.1, 1$ or 2). In these distributions, 312 values have been considered representing the maximum total number of MODIS subpixels within an OMI pixel at nadir. Cloud fractions have been included in the study by considering 31 subpixels for $c=0.1$, 62 subpixels for $c=0.2$, etc... to 281 subpixels for $c=0.9$. For the cloud simulations we have used $z=10$ km, $h=1$ km and $g=0.75$. The influence of the solar zenith angle has been tested by considering two values, $\theta_s=30^\circ$ and $\theta_s=60^\circ$. Fig. 12 illustrates the tropospheric NO₂ column error retrieved from the clear-sky part of the reflectance given by

$$R_{clear} = \frac{\langle R_{TOA} \rangle - cR_{cloud}(\langle \tau \rangle, g, z, h)}{1 - c}, \quad (7)$$

where $\langle R_{TOA} \rangle$ is the mean TOA reflectance calculated as the average of TOA reflectances calculated using Eq. (3) for the different values of the cloud optical depth distribution. The tropospheric NO₂ column error resulting from the use of a mean cloud optical depth is either positive or negative. The error remains negative for $\langle \tau \rangle=0.5$ (dotted-dashed lines) and remains positive for $\langle \tau \rangle=2$ (dashed lines). Interestingly, the error is negative for $\langle \tau \rangle=1$ (full lines) if $\theta_s=30^\circ$ and positive if $\theta_s=60^\circ$ showing the importance of the solar zenith angle in the subpixel inhomogeneity consideration. If $\theta_s=30^\circ$ or 60° , errors caused by the use of a mean cloud optical depth are expected to be less than $\pm 15\%$ for $c \leq 0.5$. For cloud fractions greater than 0.5, errors increase quickly with cloud fraction and strongly with variances and cloud optical depth. The increase of errors with cloud fraction is

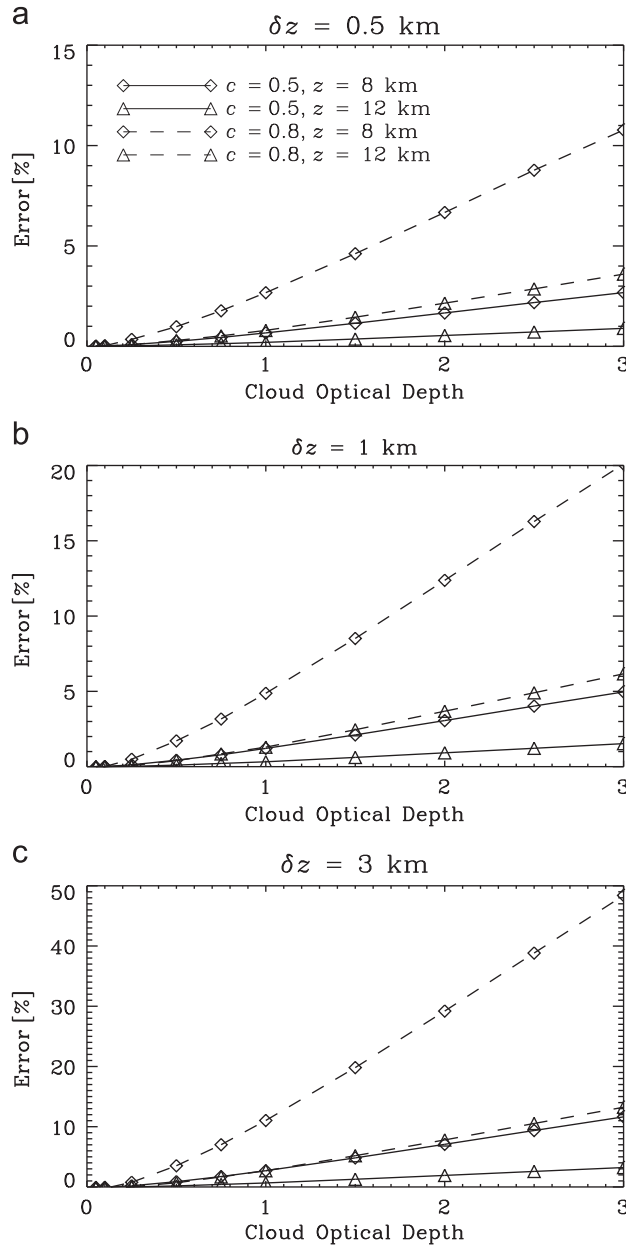


Fig. 11. NO₂ tropospheric column error caused by an uncertainty in the cloud top height (a) $\delta z = 0.5$ km, (b) $\delta z = 1$ km and (c) $\delta z = 3$ km versus cloud optical depth and for $c = 0.5$ (full lines), $c = 0.8$ (dashed lines), $z = 8$ km (diamonds) and $z = 12$ km (triangles). Here, $h = 1$ km and $g = 0.75$ and moderate polluted condition is assumed.

explained by the denominator $1 - c$ in Eq. (7). The blow-up of errors at $\text{SZA} = 60^\circ$ is explained by the bias between R_{cloud} calculated with the distribution of subpixels cloud optical depth and calculated with the mean cloud optical depth. This bias increases with the variability of cloud optical depths and solar zenith angle [59].

Finally, when the cloud fraction is lower than 0.5, the subpixel variability of the cloud optical depth does not need to be included in the cloud correction scheme. Otherwise, the subpixel variability of the cloud optical depth is significant and should be considered in the cloud

correction scheme. Such information can be deduced from MODIS observations.

6. Conclusion

In this study, we have theoretically demonstrated the sensitivity of tropospheric NO₂ column (V_{tr}) retrieval to the presence of cirrus clouds. In order of importance, we concluded that c (cloud fraction), τ (cloud optical depth), g (asymmetry factor of ice crystal phase function) and

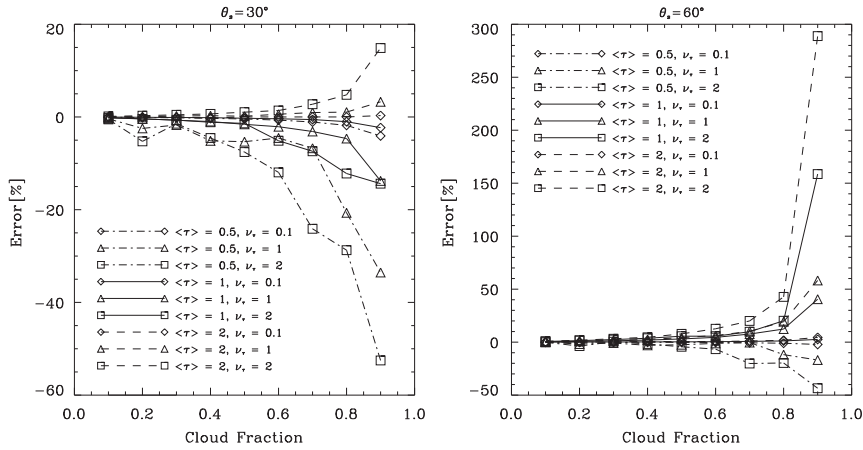


Fig. 12. NO₂ tropospheric column error caused by the use of a mean cloud optical depth instead of subpixels information versus cloud fraction if $\theta_s=30^\circ$ (left) and if $\theta_s=60^\circ$ (right).

z (cloud top height) influence the retrieval of V_{tr} . It appears from our simulations that V_{tr} is less influenced by h (cloud geometrical depth). The error on the retrieved tropospheric NO₂ column depends also on the NO₂ profile. Because tropospheric NO₂ is generally situated underneath the cirrus cloud, the shielding effect leads to underestimating the tropospheric NO₂ columns for retrievals that do not correct for clouds in the first place. The underestimation depends strongly on c and τ ranging from few percents for low cloud fraction to 55% for $c=1$ in heavily polluted conditions (i.e. for $V_{tr}=9.36 \times 10^{15}$ mol/cm²). In the context of the A-Train constellation, the tropospheric NO₂ column in presence of cirrus clouds can be retrieved by using the independent pixel approximation. The MODIS sensor coupled with CALIOP should be able to describe the optical and physical properties of the clouds in such way to reduce the error on the tropospheric NO₂ column. The use of CALIOP information is however limited by the fact that CALIOP only overlaps with the nadir pixel of OMI. Nevertheless, errors on cloud properties will end up by errors on tropospheric NO₂ column retrieval. From our simulations, we have demonstrated that the error will be reduced significantly if $c \leq 0.5$ as opposed to a retrieval that does not correct for cirrus. In the case of a cirrus cloud correction based on IPA, c and τ would have to be known within accuracy better than 0.05 and 50%, respectively. z would have to be known within accuracy of at least 1 km and g would have to be known within accuracy better than 0.05. The latter result shows that the uncertainty of the asymmetry factor is a major source of error in tropospheric NO₂ retrieval in the presence of cirrus. Using the subpixel information from MODIS cloud flag for c , from MODIS and CALIOP cloud products for τ and z and from MODIS R_{eff} for the phase function should be sufficient to reduce the error on tropospheric NO₂ column retrieval. Under this circumstance, the use of a mean value of the cloud optical depth from subpixel information as provided by MODIS should be enough to take into account the cirrus cloud and speed up the retrieval significantly. If the cloud fraction is

greater than 0.5, the subpixel variability of the cloud optical depth has to be included in the cloud correction scheme and can be obtained from MODIS. Moreover, differences between radiative transfer models used for cloud retrievals and sensor's calibration issues would introduce some discrepancies in the cloud correction scheme. The results in this study hold for retrievals that do not attempt to correct for cirrus clouds. Current state-of-science retrievals do correct for clouds that include a range of situations including cirrus clouds. Nevertheless, the current NO₂ algorithm have not be evaluated in presence of cirrus. To interpret our results in the context of current retrieval algorithms, the sensitivity for cirrus clouds in the O₂–O₂ (OMI) and O₂–A (GOME(-2), SCIAMACHY) band based cloud retrievals needs to be studied. Such studies could point out whether a correction for cirrus based on concurrent A-Train cloud information would be useful.

Acknowledgements

The authors are grateful to Céline Cornet, Philippe Dubuisson and Nicolas Ferlay from the Laboratoire d'Optique Atmosphérique (LOA) for fruitful discussions. Authors are also grateful to Christophe Goubeyre, Guillaume Mioche and Jean-François Gayet from the Laboratoire de Météorologie Physique (LaMP) for providing data from the CIRCLE-2 campaign. This research was supported by the Centre National d'Etudes Spatiales (CNES) and the Institut National des Sciences de l'Univers (INSU/PNTS).

References

- [1] Crutzen PJ. The role of NO and NO₂ in the chemistry of the troposphere and stratosphere. *Ann Rev Earth Planet Sci* 1979;7:443–72.
- [2] Solomon S, Portmann RW, Sanders RW, Daniel JS, Madsen W, Bartram, B, et al. On the role of nitrogen dioxide in the absorption of solar radiation. *J Geophys Res* 1999;104:D1012,047.

- [3] Burrows JP, Weber M, Buchwitz M, Rozanov V, Ladstätter-Weissenmayer A, Richter A, et al. The global ozone monitoring experiment (GOME): mission concept and first scientific results. *J Atmos Sci* 1999;56:151–75.
- [4] Bovensmann H, Burrows JP, Buchwitz M, Frerick J, Noël S, Rozanov VV, et al. SCIAMACHY: mission objectives and measurement modes. *J Atmos Sci* 1999;56:127–50.
- [5] Levelt PF, Hilsenrath E, Leppelmeier GW, Van den Oord GHJ, Bhartia PK, Tamminen J, et al. Science objectives of the ozone monitoring instrument. *IEEE Trans Geosci Remote Sensing* 2006;44:1199–208.
- [6] Platt U, Stutz J. Differential optical absorption spectroscopy (DOAS): principles and applications. Heidelberg, Germany: Springer; 2006.
- [7] Beirle S, Platt U, Wenig M, Wagner T. Weekly cycle of NO₂ by GOME measurements: a signature of anthropogenic sources. *Atmos Chem Phys* 2003;3:2225–32.
- [8] Richter A, Burrows JP, Nüß H, Granier C, Niemeier U. Increase in tropospheric nitrogen dioxide over China observed from space. *Nature* 2005;437:129–32.
- [9] Martin RV, Sioris CE, Chance K, Ryerson TB, Bertram TH, Wooldrige PJ, et al. Evaluation of space-based constraints on global nitrogen oxide emissions with regional aircraft measurements over and downwind of eastern North America. *J Geophys Res* 2006;111:D15308.
- [10] Boersma KF, Jacob DJ, Eskes HJ, Pinder RW, Wang J, van der ARJ. Intercomparison of SCIAMACHY and OMI tropospheric NO₂ columns: observing the diurnal evolution of chemistry and emissions from space. *J Geophys Res* 2008;113:D16526.
- [11] Celarier EA, Brinksma EJ, Gleason JF, Veefkind JP, Cede A, Herman JR, et al. Validation of Ozone Monitoring Instrument nitrogen dioxide columns. *J Geophys Res* 2008;113:D15515.
- [12] Wenig MO, Cede AM, Bucsela EJ, Celarier A, Boersma KF, Veefkind JP, et al. Validation of OMI tropospheric NO₂ column densities using direct-Sun mode Brewer measurements at NASA Goddard Space Flight Center. *J Geophys Res* 2008;113:D16545.
- [13] van Noije TPC, Eskes HJ, Dentener FJ, Stevenson DS, Ellingsen K, Schultz MG, et al. Multi-model ensemble simulations of tropospheric NO₂ compared with GOME retrievals for the year 2000. *Atmos Chem Phys* 2006;6:2943–79.
- [14] Blond N, Boersma KF, Eskes HJ, van der ARJ, Van Roozendaal M, De Smedt I, et al. Intercomparison of SCIAMACHY nitrogen dioxide observations, in situ measurements and air quality modeling results over Western Europe. *J Geophys Res* 2007;112:D10311.
- [15] Bucsela EJ, Perring AE, Cohen RC, Boersma KF, Celarier A, Gleason F, et al. Comparison of tropospheric NO₂ from in situ aircraft measurements with near-real-time and standard product data from OMI. *J Geophys Res* 2008;113:D16531.
- [16] Boersma KF, Eskes HJ, Brinksma EJ. Error analysis for tropospheric NO₂ retrieval from space. *J Geophys Res* 2004;109:D04311.
- [17] Krijger JM, van Weele M, Aben I, Frey R. Technical note: the effect of sensor resolution on the number of cloud-free observations from space. *Atmos Chem Phys* 2007;7:2881–91.
- [18] Koelemeijer R, Stammes P. Effects of clouds on ozone column retrieval from GOME UV measurements. *J Geophys Res* 1999;104:8281–94.
- [19] Liu X, Newchurch MJ, Loughman R, Bhartia PK. Errors resulting from assuming opaque Lambertian clouds in TOMS ozone retrieval. *JQSRT* 2004;85:337–65.
- [20] Kokhanovsky AA, Mayer B, Rozanov VV, Wapler K, Lamsal LN, Weber M, et al. Satellite ozone retrieval under broken cloud conditions: an error analysis based on Monte Carlo simulations. *IEEE Trans Geosci Remote Sensing* 2007;45:187–94.
- [21] Kokhanovsky AA, Rozanov VV. The uncertainties of satellite DOAS total ozone retrieval for a cloudy sky. *Atmos Res* 2008;87:27–36.
- [22] Stammes P, Sneeep M, de Haan JF, Veefkind JP, Wang P, Levelt PF. Effective cloud fractions from the Ozone Monitoring Instrument: theoretical framework and validation. *J Geophys Res* 2008;113:D16538.
- [23] Wang P, Stammes P, Boersma KF. Impact of effective cloud fraction assumption on tropospheric NO₂ retrievals. In: Proceedings of the atmospheric science conference, 8–12 May 2006 at ESRIN, Frascati Italy. Edited by H. Lacoste and L. Ouwehand. European Space Agency, 2006;SP-628:72.1.
- [24] Acarreta JR, De Haan JF, Stammes P. Cloud pressure retrieval using the O₂–O₂ absorption band at 477 nm. *J Geophys Res* 2004;109:D05204.
- [25] van Diedenhoven B, Hasekamp OP, Landgraf J. Retrieval of cloud parameters from satellite-based reflectance measurements in the ultraviolet and the oxygen A-band. *J Geophys Res* 2007;112:D15208.
- [26] Platnick S, King MD, Ackerman SA, Menzel WP, Baum BA, Riedi JC, et al. The MODIS cloud products: algorithms and examples from Terra. *IEEE Trans Geosci Remote Sensing* 2003;41:459–73.
- [27] Wylie DP, Menzel WP, Woolf HM, Strabala KI. Four years of global cirrus cloud statistics using HIRS. *J Clim* 1994;7(12):1972–86.
- [28] Nazaryan H, McCormick MP, Menzel WP. Global characterization of cirrus clouds using CALIPSO data. *J Geophys Res* 2008;113:D16211.
- [29] Kleipool QL, Dobber MR, de Haan JF, Levelt PF. Earth surface reflectance climatology from 3 years of OMI data. *J Geophys Res* 2008;113:D18308.
- [30] Rozanov AA, Rozanov VV, Buchwitz M, Kokhanovsky AA, Burrows JP. SCIATRAN 2.0—a new radiative transfer model for geophysical applications in the 175–2400 nm spectral range. *Adv Space Res* 2005;36:1015–9.
- [31] Boersma KF, Eskes HJ, Veefkind JP, Brinksma EJ, van der ARJ, Sneeep M, et al. Near-real time retrieval of tropospheric NO₂ from OMI. *Atmos Chem Phys* 2007;7:2103–18.
- [32] Pfeilsticker K, Erle F, Funk O, Marquard L, Wagner T, Platt U. Optical path modifications due to tropospheric clouds: implications for zenith sky measurements of stratospheric gases. *J Geophys Res* 1998;103(D19):25323–35.
- [33] Oshchepkov S, Isaka H, Gayet JF, Sinyuk A, Auriol F, Havemann S. Microphysical properties of mixed-phase and ice clouds retrieved from in situ airborne “Polar Nephelometer” measurements. *Geophys Res Lett* 2000;27:209–13.
- [34] Jourdan O, Oshchepkov S, Shcherbakov V, Gayet JF, Isaka H. Assessment of cloud optical parameters in the solar region: retrievals from airborne measurements of scattering phase functions. *J Geophys Res* 2003;108:D134572.
- [35] Yang P, Liou KN. Geometric-optics-integral-equation method for light scattering by nonspherical ice crystals. *Appl Opt* 1996;35:6568–84.
- [36] Shcherbakov VN, Gayet JF, Jourdan O, Minikin A, Ström J, Petzold A. Assessment of cirrus cloud optical and microphysical data reliability by applying statistical procedures. *J Atmos Ocean Technol* 2005;22:409–20.
- [37] Gayet JF, Shcherbakov VN, Mannstein H, Minikin A, Schumann U, Ström J, et al. Microphysical and optical properties of midlatitude cirrus clouds observed in the southern hemisphere during INCA. *QJR Meteorol Soc* 2006;132:2719–48.
- [38] Francis PN, Foot JS, Baran AJ. Aircraft measurements of the solar and infrared radiative properties of cirrus and their dependence on ice crystal shape. *J Geophys Res* 1999;104:31685–96.
- [39] Labonnote LC, Brogniez G, Buriez JC, Doutriaux-Boucher M, Gayet JF, Macke A. Polarized light scattering by inhomogeneous hexagonal monocrystals: validation with ADEOS-POLDER measurements. *J Geophys Res* 2001;106:12139–54.
- [40] Baran AJ, Francis PN. On the radiative properties of cirrus cloud at solar and thermal wavelengths: a test of model consistency using high-resolution airborne radiance measurements. *QJR Meteorol Soc* 2004;130:763–78.
- [41] Baran AJ, Labonnote LC. On the reflection and polarisation properties of ice cloud. *JQSRT* 2006;100:41–54.
- [42] Baran AJ, Labonnote LC. A self-consistent scattering model for cirrus. I: the solar region. *QJR Meteorol Soc* 2007;133:1899–912.
- [43] Bucsela EJ, Celarier EA, Wenig MO, Gleason JF, Veefkind JP, Boersma KF, et al. Algorithm for NO₂ vertical column retrieval from the ozone monitoring instrument. *IEEE Trans Geosci Remote Sensing* 2006;44:1245–58.
- [44] Boersma KF, Dirksen R, Veefkind JP, Eskes HJ, van der ARJ. Dutch OMI NO₂ (DOMINO) data product HE5 data file user manual, TEMIS website, <<http://www.temis.nl/airpollution/no2.html>>, 2008.
- [45] Dufour E, Bréon FM. Spaceborne estimate of atmospheric CO₂ column by use of the differential absorption method: error analysis. *Appl Opt* 2003;42:3595–609.
- [46] Schneising O, Buchwitz M, Burrows JP, Bovensmann H, Reuter M, Notholt J, et al. Three years of greenhouse gas column-averaged dry air mole fractions retrieved from satellite—part 1: carbon dioxide. *Atmos Chem Phys* 2008;8:3827–53.
- [47] Yang P, Liou KN. Single-scattering properties of complex ice crystals in terrestrial atmosphere. *Contr Atmos Phys* 1998;71:223–48.
- [48] Koelemeijer R, Stammes P, Hovenier J, de Haan J. A fast method for retrieval of cloud parameters using oxygen a band measurements from the global ozone monitoring experiment. *J Geophys Res* 2001;106(D4):3475–90.
- [49] Koren I, Oreopoulos L, Feingold G, Remer LA, Altartatz O. How small is a small cloud?. *Atmos Chem Phys* 2008;8:3855–64.
- [50] Mace GG, Zhang Y, Platnick S, King MD, Minnis P, Yang P. Evaluation of cirrus cloud properties derived from MODIS data using cloud

- properties derived from ground-based observations collected at the ARM SGP site. *J Appl Meteor* 2005;44:221–40.
- [51] Ackerman SA, Holz RE, Frey R, Eloranta EW, Maddux BC, McGill M. Cloud detection with MODIS. Part II: validation. *J Atmos Oceanic Technol* 2008;25:1073–86.
- [52] Winker DM, Pelon JR, McCormick MP. The CALIPSO mission: spaceborne lidar for observation of aerosols and clouds. *Proc SPIE* 2003;4893:1–11.
- [53] Baran AJ. A review of the light scattering properties of cirrus. *JQSRT* 2009;110:1239–60.
- [54] Garrett TJ, Hobbs P, Gerber H. Shortwave, single-scattering properties of arctic ice clouds. *J Geophys Res* 2001;106(D14):15155–72.
- [55] Gayet JF, Asano S, Yamazaki A, Uchiyama A, Sinyuk A, Jourdan, O, et al. Two case studies of winter continental-type water and mixed-phase stractocumuli over the sea, part I: microphysical and optical properties. *J Geophys Res* 2002;107:D214569.
- [56] Baum BA, Heymsfield AJ, Yang P, Bedka ST. Bulk scattering models for the remote sensing of ice clouds. Part 1: microphysical data and models. *J Appl Meteor* 2005;44:1885–95.
- [57] Baum BA, Yang P, Heymsfield AJ, Platnick S, King MD, Hu, YX, et al. Bulk scattering models for the remote sensing of ice clouds. Part 2: narrowband models. *J Appl Meteor* 2005;44:1896–911.
- [58] Chiriaco M, Chepfer H, Minnis P, Haeffelin M, Platnick S, Baumgardner, D, et al. Comparison of CALIPSO-like, LaRC, and MODIS retrievals of ice-cloud properties over SIRTa in France and Florida during CRYSTAL-FACE. *J Appl Meteor Clim* 2007;46:249–72.
- [59] Cahalan RF, Ridgway W, Wiscombe WJ, Bell TL, Snider JB. The albedo of fractal stratocumulus clouds. *J Atmos Sci* 1994;51:2434–55.